chemosensors

MDPI

Article

Fluorescent Calix[4]arene-Carbazole-Containing Polymers as Sensors for Nitroaromatic Explosives

Patrícia D. Barata [1,2] and José V. Prata [1,2,*]

[1] Departamento de Engenharia Química, Instituto Superior de Engenharia de Lisboa, Instituto Politécnico de Lisboa, R. Conselheiro Emídio Navarro, 1, 1959-007 Lisboa, Portugal; pbarata@deq.isel.ipl.pt

[2] Centro de Química-Vila Real, Universidade de Trás-os-Montes e Alto Douro, 5001-801 Vila Real, Portugal

* Correspondence: jvprata@deq.isel.ipl.pt; Tel.: +351-218-317-172

Received: 30 October 2020; Accepted: 8 December 2020; Published: 10 December 2020

Abstract: Two highly fluorescent calix[4]arene-containing phenylene-*alt*-ethynylene-carbazolylene polymers (Calix-PPE-CBZs) were used in the detection of explosives from the nitroaromatic compounds (NACs) family, in solution and in vapour phases. Both fluorophores exhibit high sensitivity and selectivity towards NACs detection. The quenching efficiencies in solution, assessed through static Stern-Volmer constants (K_{SV}), follow the order picric acid (PA) >> 2,4,6-trinitrotoluene (TNT) > 2,4-dinitrotoluene > (2,4-DNT) > nitrobenzene (NB). These correlate very well with the NACs electron affinities, as evaluated from their lowest unoccupied molecular orbitals (LUMOs) energies, indicating a photo-induced electron transfer as the dominant mechanism in fluorescence quenching. Moreover, and most interesting, detection of TNT, 2,4-DNT and NB vapours via thin-films of Calix-PPE-CBZs revealed a remarkably sensitive response to these analytes, comparable to state-of-the-art chemosensors. The study also analyses and compares the current results to previous disclosed data on the detection of NACs by several calix[4]arene-based conjugated polymers and non-polymeric calix[4]arenes-carbazole conjugates, overall highlighting the superior role of calixarene and carbazole structural motifs in NACs' detection performance. Density functional theory (DFT) calculations performed on polymer models were used to support some of the experimental findings.

Keywords: calix[4]arene; conjugated polymer; carbazole; fluorescence; sensor; explosives

1. Introduction

Development of chemical sensors and devices thereof for trace detection of high explosives is a very active area of research given the potential of this approach to increase anti-terrorism actions and homeland security, to help foster secure methodologies for hidden landmines detection and, in general, to assist environmental and forensic investigations related to explosive materials [1–4]. Therefore, development of fast and ultra-sensitive detection devices for explosive materials is critical to ensuring global security. Nitroaromatic compounds (NACs) are important primary constituents found in many explosives compositions, particularly in military fields, and also widely employed in agrochemical, dye and pharmaceutical industries. NACs, such as 2,4,6-trinitrophenol (picric acid, PA), 2,4,6-trinitrotoluene (TNT) and 2,4-dinitrotoluene (2,4-DNT), are primary military explosives, some of them the main components in unexploded landmines worldwide, and thus have been the most targeted group of substances envisaged in the research efforts [4].

Although very precise methods exist for NACs detection and quantification, which rely on several well-established techniques (e.g., surface enhanced Raman spectroscopy (SERS), ion mobility spectrometry (IMS), gas chromatography-electron capture detection (GC/ECD) and electrospray ionization-liquid chromatography/mass spectrometry (ESI-LC/MS)), they are usually quite expensive, time-consuming and/or lack the portability required for in-field applications [5,6]. In this context,

simple, cost-effective and increasingly more sensitive and selective detection methods are needed for real-world applications. Luminescence-based methods for analyte detection are highly sensitive and have long been recognized as one of the main signal transduction techniques for chemical sensing. Since explosives in general do not fluoresce under UV-Vis irradiation, indirect fluorescence techniques using chemical sensors sensitive to their presence, either through turn-off or turn-on mechanisms of fluorescence emission, have to be employed, the former usually being used [2,7–9].

One of the most prominent areas for the application of fluorescent conjugated polymers (CPs), in particular those having aryleneethynylene repeating units in their main-chains, is as active layers in chemical sensor devices for in-field detection of NACs [10–12]. One widely studied feature of these systems is their ability to produce a signal amplification in response to interactions with analyte molecules. This concept was pioneered by Swager and Zhou [13,14] who paved the way to new sensory materials using this important CP's class. Since the first studies [15], this sort of fluorescence quenching transduction mechanism has been largely employed in explosives detection [10,11]. Many examples involving the use of poly(phenyleneethynylene)s (PPEs) [16–18], poly(phenylenevinylene)s [19,20] and polycarbazoles [21,22] can be found in the literature. Small-molecule fluorophores have also been investigated as explosive sensors [4]. Some of them may offer certain advantages over CP materials such as simpler synthesis, more well-defined structures and cost-effectiveness. Nonetheless, conjugated polymer-based sensors usually exhibit increased quenching efficiency, mainly in solid state sensor devices, due to an enhanced quenching mechanism based on excitonic migration. In these systems possessing receptors wired in series, the excitons generated upon sample irradiation, while migrating in a random fashion within the conjugated backbone, may be quenched by a single quencher molecule residing at a given receptor site, attenuating the fluorescence of the whole conjugated chain [13]. Such mechanism is not feasible with small-molecule fluorophores where the quenching is brought about on a stoichiometric basis of one analyte molecule per signalling fluorophore [2,4].

Calixarenes, in particular calix[4]arenes, are among the most investigated macrocyclic scaffolds for molecular recognition. Owing to their well-defined π-electron-rich cavity, the countless derivatives that can be prepared by upper and lower rim functionalisation and the unique properties derived from their more or less flexible or even rigid conformations, which precisely define sites for strong interactions with guest molecules or ions, calixarenes are one of the most valuable classes of synthetic molecular receptors [23–25]. The incorporation of calix[4]arene moieties in CPs has proved to be very effective in enhancing the sensory properties of polymeric systems since the bulky bowl-shaped elements not only prevent π-stacking of the polymer chains in the solid state, thus preserving the essential luminescent properties of the polymers, but also help to construct interstitial voids able to host selected guests, overall allowing the creation of highly sensitive films for explosives detection [26]. Design of highly sensitive and selective sensory materials for detection of explosives (e.g., NACs and explosive taggants), pollutants (e.g., nitroaromatic amines) and biological materials (e.g., haemoproteins) have been centred on several fluorescent calix[4]arene-based poly(aryleneethynylene)s [27–30]. In the field of explosives detection, their sensing abilities towards NACs [26,30], nitroaliphatic liquid explosives and an explosive taggant [31] have been demonstrated.

Herein, we report on the chemosensing ability of highly fluorescent calix[4]arene-containing phenylene-*alt*-ethynylene-2,7- and 3,6-carbazolylene polymers (Calix-PPE-2,7-CBZs and Calix-PPE-3,6-CBZs, respectively) (Chart 1) towards the detection of a series of nitroaromatic explosives (picric acid, 2,4,6-trinitrotoluene, 2,4-dinitrotoluene and nitrobenzene) in liquid phase as well as in vapour phase. The study, showing their noteworthy behaviour as chemosensors, will be complemented by state-of-the-art density functional theory (DFT) calculations which will help to understand some of their experimentally found performances.

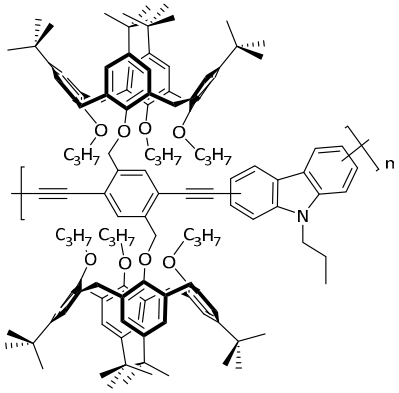

Chart 1. Chemical structure of Calix-PPE-CBZs.

2. Materials and Methods

2.1. Materials

The Calix-PPE-CBZs (Chart 1) selected for the current study were prepared according to our previous report [27]. Details pertaining their synthesis and characterisation may be found in Supplementary Materials (SM). Nitrobenzene (NB; 99%, Merck) was distilled under vacuum, 2,4-dinitrotoluene (2,4-DNT; 97%, Aldrich) was recrystallized from acetone, picric acid (PA; 99.5%, Merck) was recrystallized from chloroform, 1,4-benzoquinone (BQ; 98%, Aldrich) was recrystallized from ethanol, and benzoic acid (BA; 99%, Merck) was recrystallized from water. 2,4,6-Trinitrotoluene (TNT) was prepared from a literature procedure [32]. Hydrazine hydrate (99%, Analar) was used as received.

2.2. Instruments and Methods

UV-vis spectra were recorded on a Nicolet Evolution 300 or on a Jasco J-815 spectrophotometer using 1-cm quartz cells at 25 °C.

Steady-state fluorescence spectra were acquired on a Perkin Elmer LS45 fluorimeter using a 1-cm quartz cuvette in right angle (RA) and front-face (FF; oriented at ca. 30° relative to the incident beam) geometries at 25 °C, in air-equilibrated conditions.

Solution experiments were carried out via titration of diluted solutions of the polymers in $CHCl_3$ with known amounts of analytes using RA geometry. Inner-filter effects (IFEs) were corrected at the excitation and emission wavelengths [33]; the acquisition of absorption spectra for the entire range of quencher concentrations followed an identical titration procedure.

The extent of the developed interactions between the chemosensors and the analytes were quantified using the Stern-Volmer equation ($F_0/F = 1 + K_{SV}$ [Q]) derived from static quenching, plotting F_0/F versus [Q], where F_0 and F are the fluorescence intensities in the absence and presence of the quencher (Q), [Q] is the quencher concentration and K_{SV} is the static Stern-Volmer constant [34].

Thin-films with different thicknesses for quenching studies in solid state were prepared via spin-coating (home-made spin-coater; spin-rate of 1500 rpm) from appropriate solutions of fluorophores in $CHCl_3$ on quartz substrates (4 cm × 0.8 cm), followed by vacuum drying for 1 h before use. The average thickness of spin-casted films was determined with a Veeco Dektak 6M profilometer as described elsewhere [31]. A calibration curve was established using films with optical densities (ODs) ranging from 0.06 to 0.23 at the excitation wavelength (λ_{exc} = 360 nm), affording a linear relationship between the optical data and film thicknesses within this range (R^2 = 0.9971). For ODs < 0.06, the corresponding thicknesses were assessed via data extrapolation.

The quenching assays were performed as follows: an amount of analyte was placed in a 20 mL chamber and covered with cotton gauze; to guarantee a constant vapour pressure before the placement of the film, the closed cell was allowed to saturate for at least 16 h at 25 °C. Initial fluorescence was recorded and then the film was transferred to the saturated chamber and exposed to the analyte vapours for certain time intervals; after each exposure the fluorescence spectrum was immediately recorded. Fluorescence data were collected under FF illumination. The quenching efficiencies were determined in a time-dependent manner, using the expression $((F_0 - F)/F_0 \times 100)$, where F_0 is the initial fluorescence and F is the fluorescence after exposure to saturated vapours of explosive. The complete data set was acquired from 10 s to 15 min exposure time.

2.3. Computational Methods

Lowest-energy conformers for Calix-2-CBZ and Calix-3-CBZ (Figure S4) were first obtained from conformational searches (Monte Carlo method, MMFF94 force field) and then subjected to full energy and geometry optimisation using density functional theory (DFT) calculations running on a hybrid model (B3LYP) using the 6-31G(d) basis set, using default grids and convergence criteria in vacuum. Single point energy calculations followed, using a functional with Grimme dispersion (B3LYP-D3) and a larger basis-set (6-311+G(d,p)) to better account for London dispersion and basis set superposition errors [35]. Calculations on the conjugated structures 2,2′/3,3′-((2,5-dimethyl-1,4-phenylene)bis(ethyne-2,1-diyl))bis(9-propyl-9*H*-carbazoles (Model-Calix-CBZs; Figure S5), lacking the calixarene units, were then performed using the same strategy. By comparing the energies of the highest occupied molecular orbitals (HOMOs) and the lowest unoccupied molecular orbitals (LUMOs) of Calix-CBZs and their respective truncated models, it was verified that the HOMO/LUMO energies of the latter structures are very close to those obtained for the calixarene compounds (cf. Figures S4 and S5), thus establishing the grounds for a similar approach in the calculations of model polymers; direct calculations on Calix-PPE-CBZs are otherwise computationally not feasible.

Pentamer models of each polymer (Pentamer models-Calix-PPE-CBZs; Figures S6 and S7) were fully optimised (energy and geometry) using the B3LYP/6-31G(d) formalism and their energies further accessed using single point calculations at B3LYP-D3/6-311+G(d,p)) level. The HOMO/LUMO energy levels of all the NACs, BQ and BA used in the study were calculated similarly.

The binding energies (ΔE) in gas-phase for the complexation between Model-Calix-2-CBZ and the various analytes (PA, TNT, 2,4-DNT, NB and BQ) were calculated using the equation $\Delta E = E_{\text{Complex}} - (E_{\text{Model-Calix-2-CBZ}} + E_{\text{Analyte}})$, where E_{Complex} is the energy of the complex formed from Model-Calix-2-CBZ and a given analyte. DFT energy calculations were performed at B3LYP-D3/6-311+G(d,p) level of theory in vacuum.

All calculations were performed using Q-Chem 5.1 [36] running on Spartan'18 molecular modelling software [37].

3. Results and Discussion

3.1. Synthesis and Structural Characterisation of Calix-PPE-CBZs

The Calix-PPE-CBZs (Chart 1) used in the study were synthesized using a reported procedure [27]. They were prepared via polycondensation of bis-calix[4]arene-diiodides with 2,7/3,6-diethynyl-9-propyl-9*H*-carbazoles using a Sonogashira-Hagihara coupling reaction (Scheme S1; see SM for details), being obtained in good isolated yields (84% and 70%, respectively, for 2,7- and 3,6-isomers). Structural analysis (see SM for details; Figures S1 and S2) using FTIR and ^{1}H/^{13}C NMR spectroscopies fully confirm the assigned structures. Gel permeation chromatography (GPC) allowed the determination of the polymers' weight-average molecular weights (Figure S3), which range from 8000 g·mol^{-1} (M_w/M_n = 1.73; average degree of polymerisation (DP) ≈ 2) for

Calix-PPE-3,6-CBZ to 27,000 g·mol^{-1} (M_w/M_n = 2.99; DP ≈ 5) for Calix-PPE-2,7-CBZ, determined against polystyrene standards.

3.2. Solution Quenching Studies

The evaluation of the sensory properties displayed by Calix-PPE-CBZs in solution was carried out via the quantification of their emission intensity variations in the presence of selected NACs (PA, TNT, 2,4-DNT and NB).

Figure 1 presents the emission spectra of Calix-PPE-2,7-CBZ in $CHCl_3$ obtained after successive additions of a TNT solution in a concentration range of 7.40 × 10^{-5} to 8.26 × 10^{-4} M, keeping the concentration of the polymer constant (6.0 × 10^{-7} M). While the apparent quenching constants may be retrieved from direct plotting of emission intensities (inset (a), Figure 1), they need to be corrected for primary and secondary IFEs resulting from the absorption of radiation at the excitation (360 nm) and emission wavelengths (430 nm for Calix-PPE-2,7-CBZ and 403 nm for Calix-PPE-3,6-CBZ) by the analytes (cf. UV-Vis spectra of NACs in Figure S11) in order to get more accurate static Stern-Volmer constants (K_{SV}). This was done by following a reported procedure [33], leading to the new plot shown in Figure 1, inset (b). Unfortunately, correction of IFEs is not always followed in literature reports, which, not uncommonly, may lead to overestimated results of a sensor performance.

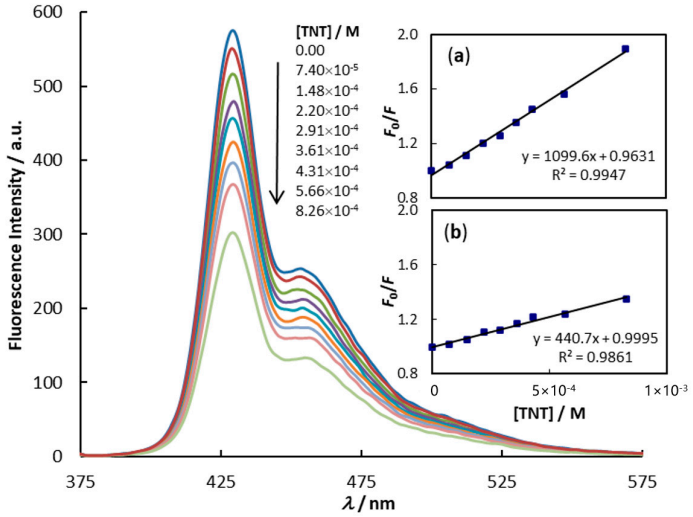

Figure 1. Emission spectra of Calix-PPE-2,7-CBZ (6.0 × 10^{-7} M in $CHCl_3$) after successive additions of 2,4,6-trinitrotoluene (TNT) (λ_{exc} = 360 nm). Inset: Stern-Volmer uncorrected (**a**) and corrected (**b**) plots.

An identical approach was followed for the other NACs (PA, 2,4-DNT and NB; Figures S12–S14). In the case of PA, given the strong deviation from linearity observed in the concentration range used for the other NACs, the study was performed at an order of magnitude lower (7.40 × 10^{-6} to 5.66 × 10^{-5} M). Similar experiments and correction procedures were carried out with Calix-PPE-3,6-CBZ for the various analytes. Table 1 gathers the findings.

Table 1. Corrected Stern-Volmer constants for Calix-PPE-CBZs with nitroaromatic compounds (NACs) (K_{sv}/M^{-1}).

Analyte [1]	PA	TNT	2,4-DNT	NB
Calix-PPE-2,7-CBZ	3431	441	220	108
Calix-PPE-3,6-CBZ	3628	386	264	109

[1] Concentration range: 7.40 × 10^{-5}–8.26 × 10^{-4} M, except for picric acid (PA) (7.40 × 10^{-6}–5.66 × 10^{-5} M), in $CHCl_3$ solution; λ_{exc} = 360 nm.

A great affinity of Calix-PPE-CBZs for PA can be immediately perceived from the above data. For the other NACs under study, the quenching abilities follow the order TNT > 2,4-DNT > NB. Following the 3σ IUPAC criteria [38], the limit of detection (LOD) of each NAC was determined (Table S1). Calix-PPE-2,7-CBZ stands out as the best sensory material for all the analytes. The lowest LOD in $CHCl_3$ solution was achieved for PA (0.77 ppm), followed by TNT (6.0 ppm), DNT (9.6 ppm) and NB (13.2 ppm). This behaviour may be correlated with the electron affinities of NACs. Indeed, fluorescent detection of electro-deficient NACs by electron-donating species, such as conjugated polymers, typically involves an oxidative photo-induced electron transfer (PET) mechanism [4]. Upon light excitation, an electron transfer ensues from the excited state of the fluorophore (mainly located in the PPE-CBZ chains) to the LUMO of the NAC, followed by a non-radiative electron transfer to the ground state of the fluorophore resulting in fluorescence quenching (Figure S8). The larger the energy gap between the two states of the donor-acceptor pair, the more exergonic the electron transfer is, resulting in more favourable PETs.

To gain further insight into the above reasonings, models of Calix-PPE-CBZs simulating their main chain repeating units and linkages were constructed. The energy and geometry of the pentamer models (Pentamer models-Calix-PPE-CBZs; Figures S6 and S7) were first optimised using DFT calculations at B3LYP/6-31G(d) level of theory and then by a single point energy calculation using the Grimme dispersion model (B3LYP-D3) [35] and a larger basis-set (6-311+G(d,p)) (see details in Materials and Methods section). The LUMOs energies calculated for the pentamer models of Calix-PPE-2,7-CBZ and Calix-PPE-3,6-CBZ are −2.39 eV and −1.87 eV, respectively, whereas the NACs' LUMOs energies are −4.42 eV ($E_{LUMO(PA)}$), −3.99 eV ($E_{LUMO(TNT)}$), −3.48 eV ($E_{LUMO(2,4\text{-}DNT)}$) and −2.96 eV ($E_{LUMO(NB)}$). First, for all the NACs, the electron transfer is thermodynamically allowed from the singlet excited state of polymers to the NACs LUMOs (Figure S9); contrary to this, PET is not allowed for benzoic acid ($E_{LUMO(BA)}$ = −1.84 eV; Figure S9), a fact that was experimentally evidenced by the absence of any response in fluorescence titration experiments (Figure S15). Secondly, the higher driving force for the electron transfer comes from the highest electron-deficient PA, followed by TNT, 2,4-DNT and finally NB. This is precisely the order found in the quenching experiments. Differences in the LUMOs energies of the two polymers' isomers (models) are due to the different extent of π-conjugation along the main chain. A longer conjugation length of 2,7-PPE-CBZ isomer lowers its LUMO energy in comparison to the 3,6-homolog, as well as the HOMO-LUMO gap resulting in a red-shift absorption and emission [27]. That is to say that, solely based on the LUMOs/singlet excited state energies of the donors, one should expect a higher affinity of NACs for the 3,6-isomer. Again, this was experimentally observed in the fluid phase for PA and 2,4-DNT. Differences observed for the other NACs are less clear due to the proximal K_{SV}. Another point that should be noted is that, at least in solution, a signal amplification effect due to exciton migration along the polymer chain, which would favour the 2,7-PPE-CBZ isomer, is apparently not discernible.

For comparison and benchmarking, 1,4-benzoquinone (BQ) was used as a model for strong non-aromatic/non-nitrated electron-deficient species. Although its LUMO energy ($E_{LUMO(BQ)}$ = −3.99 eV) is identical to that of TNT, a considerably higher affinity for the latter was found in the quenching assays. Indeed, using Calix-PPE-2,7-CBZ as the fluorophore, the K_{SV} for BQ reaches only 217 M^{-1} (Figure S16), which is less than half that obtained for TNT. A similar trend was observed for Calix-PPE-3,6-CBZ, where the corresponding K_{SV} for BQ was 122 M^{-1}. These results illustrate that besides an allowed electron transfer process other factors control the extent of the quenching and thus the magnitude of K_{SV}. In the present case, it seems plausible to consider that less strong electrostatic interactions exist between BQ and the main transduction sites in the polymer chain (phenylene-ethynylene-carbazolylene repeating units) in comparison to TNT. The binding energy of such ground state interactions was tentatively accessed by modelling the formation of a complex between the analytes and the fluorogenic system. A previous sift for energy-minimised structures of Calix-2-CBZ-TNT complexes using a molecular mechanics approach (equilibrium geometries obtained from MMFF94 force field) pointed to an assemble where the analyte resides near the carbazole unit; thus, all the input geometries of the complexes for energy and geometry-optimised structures using DFT calculations started with such a type of molecular arrangement. To reduce computational costs, the truncated Calix-2-CBZ structure

was used as a model for the polymer. The structure of the complexes formed are displayed in Figure S10. Table 2 shows the binding energies (ΔE) obtained for all the NACs and BQ. The results clearly indicate a preference for PA, followed by TNT > 2,4-DNT > BQ > NB, which qualitatively agree with the magnitudes of the K_{sv} experimentally found.

Table 2. Binding energy (ΔE) in gas-phase for the complexation between Model-Calix-2-CBZ and various analytes [1].

Analyte	ΔE/kJ·mol^{-1}
PA	−84.0921
TNT	−75.3203
2,4-DNT	−57.8634
NB	−40.4957
BQ	−49.4434

[1] Density functional theory (DFT) energy calculations were performed at B3LYP-D3/6-311+G(d,p) level of theory in vacuum [36,37].

To highlight how structural and/or electronic features present in several calixarene systems might govern the outcome of NACs-sensing events, two conjugated polymers, Calix-*p*-PPE [28,39] and Calix-OCP-PPE [30,40] (Chart 2a,b), and non-polymeric (Calix-CBZs) [41] (Chart 2c) calixarene sensors, previously disclosed by our research group, were compared. Their detection abilities are shown in Figure 2. The former two have in common the phenylene-*alt*-ethynylene conjugated system but distinct arrangements of calixarene units along the polymer chain, while the latter ones possess structurally identical fluorogenic elements to that of Calix-PPE-CBZs but short conjugation lengths.

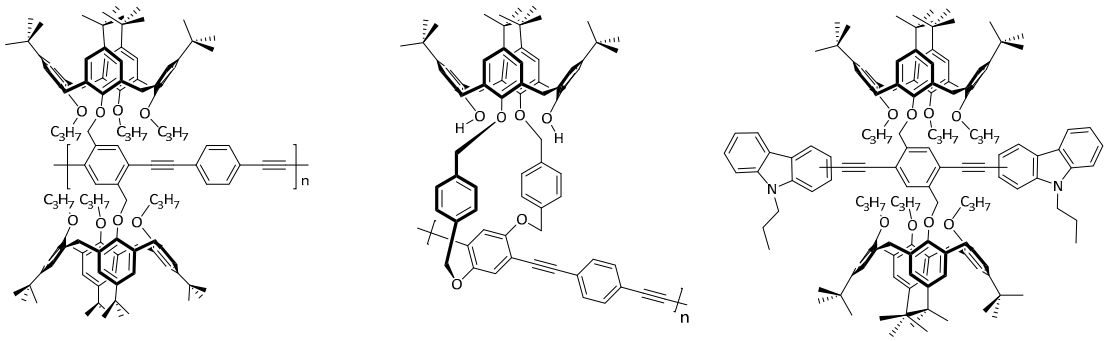

Chart 2. Chemical structures of Calix-*p*-PPE (**a**), Calix-OCP-PPE (**b**) and Calix-CBZs (**c**).

The results in Figure 2 show, in general, a greater sensitivity of Calix-PPE-CBZs in NACs detection, particularly for picric acid, as compared to the other PPEs, highlighting the role of carbazole moieties in attaining strong electrostatic interactions with the NACs.

When the sensitivities of Calix-PPE-CBZs and Calix-CBZs are compared, a higher sensory response to PA is found for either polymer systems; for TNT, the results also slightly favours the polymer sensors, while for the less electron-deficient 2,4-DNT and NB a higher quenching efficiency was observed for Calix-CBZs. A higher selectivity of Calix-PPE-CBZs for TNT, compared to the non-polymer analogues, may also be understood from the inset of Figure 2.

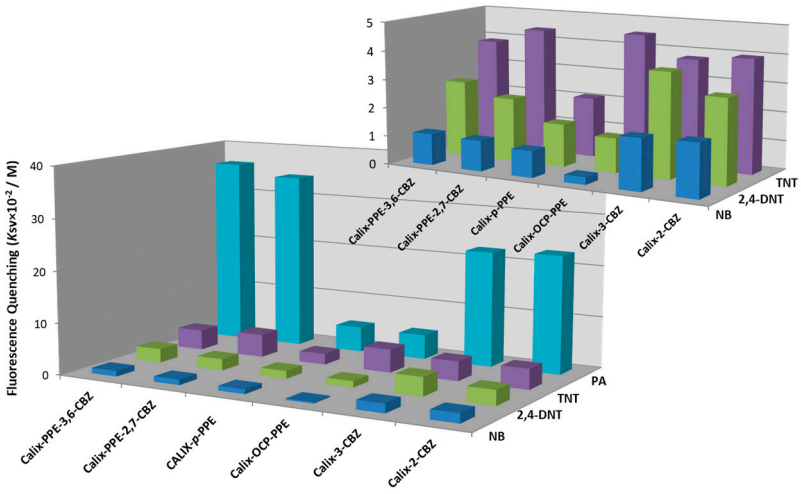

Figure 2. Fluorescence quenching (corrected K_{SV}) of Calix-PPE-CBZs (λ_{exc} = 360 nm), Calix-*p*-PPE and Calix-OCP-PPE (λ_{exc} = 380 nm), and Calix-CBZs (λ_{exc} = 360 nm) by NACs in $CHCl_3$ solution. Inset: expanded data for TNT, 2,4-DNT and NB analytes.

3.3. Solid State Quenching Studies

The aforementioned results revealed a high efficiency and selectivity of Calix-PPE-CBZs towards the detection of several explosive compounds in liquid phase. Although detection of explosives in liquid phase has some important uses, for example in forensic and environmental analysis [42], vapour phase detection using sensory materials in solid state is particularly important for in-field applications. The capacity to form stable thin-films, either on their own or incorporated in a polymeric support, a high photostability and a substantial fluorescence quantum yield are all essential features required for practical uses of such materials in sensing devices. On the other hand, the low vapour pressures of most explosives at room temperature makes their detection in air a challenging task.

In the following, the ability of the two Calix-PPE-CBZs to work as solid state chemosensors for selected nitroaromatics (TNT, 2,4-DNT and NB) in vapour phase is scrutinized. The extremely low vapour pressure of PA (0.971 ppb) [43] precluded its use in the assays. A static setup was employed in the assays (details may be found in the Materials and Methods section). Polymer films were prepared by spin-coating their $CHCl_3$ solutions onto a quartz substrate. Dried films were then exposed to the analyte vapours for a certain time and the fluorescence emission consecutively measured. Figure 3a–c show the emission intensities of Calix-PPE-2,7-CBZ films (thicknesses ≈ 20 nm) upon exposure to the different NACs' vapours over time (10 s to 15 min), under front-face illumination. The corresponding fluorescence quenching efficiencies are depicted in Figure 3d. The results retrieved for the three analytes clearly point to a considerable efficacy in NACs detection. Slightly different responses were observed for Calix-PPE-3,6-CBZ with the same analytes (Figure S17), but overall, the same trend was followed. Indeed, strong and quick responses to NB (93 and 86% for Calix-PPE-3,6-CBZ and Calix-PPE-2,7-CBZ, respectively) and 2,4-DNT (62 and 66% for the same polymers) were observed in only 30 s of exposure, reaching values near 88-94% for NB and 68-76% for 2,4-DNT by both polymers after a one minute of exposure. For TNT, slower responses were found (less than 20% upon one minute of contact). Stronger quenching activity was only observed after prolonged exposures (e.g., 15 min), with 74 and 69% quenching efficiencies for 3,6-CBZ and 2,7-CBZ polymers, respectively.

As already mentioned, the fluorescence quenching mechanism underlying the interaction between electron-donating CPs and electro-deficient NACs involves an oxidative PET. When assessing the extent of quenching of emission in solid state matrices by vapours of explosives, several other factors need to be considered. Actually, besides the PET exergonicity, the vapour pressure of the analyte (its concentration under the assay conditions), the thickness of the sensor films and their morphology

and the strongness of the electrostatic interactions developed between the fluorescent materials and the quencher are additional parameters that should be tackled in [13,44].

The vapour pressures of the NACs under study are 2.42×10^{-1} mmHg for NB at 23 °C [45], 1.44×10^{-4} mmHg for 2,4-DNT [46] and 8.02×10^{-6} mmHg for TNT [46] at 25 °C, which translate into 318 ppm, 190 ppb and 10 ppb, respectively, as the equilibrium concentrations of the NACs under the conditions of the experiments. As a corollary, the quicker responses found for NB and 2,4-DNT, in comparison to TNT, largely reside on their higher volatility. When further compared to BQ, an oxidant having a similar electron affinity as TNT (cf. LUMO energies above) but a huge vapour pressure (1.74×10^{-1} mmHg, 229 ppm, at 25 °C) [47], a very rapid response was registered (around 90% of quenching for both PPE-CBZ polymers after 30 s; Figure S18), again highlighting the strong impact of the analyte vapour pressure on the quenching behaviour. On the other hand, one can undoubtedly attribute the highest quenching power to TNT, despite the slower response shown. Indeed, since its concentration under the experimental conditions used is more than 3.2×10^4, 2.3×10^4, and 19 times less than that of NB, BQ and 2,4-DNT, respectively, the relative magnitude of the obtained quenching efficiencies are far from those figures.

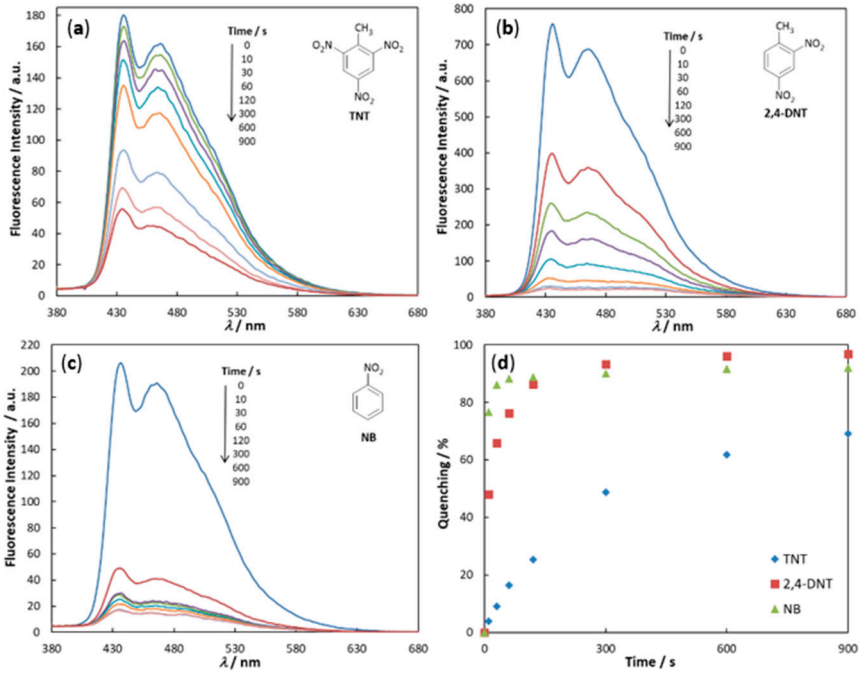

Figure 3. Time-dependent emission intensities (**a**–**c**) and fluorescence quenching efficiencies (**d**) of Calix-PPE-2,7-CBZ films (≈20 nm) after being exposed to saturated TNT (10 ppb) (**a**), 2,4-DNT (190 ppb) (**b**) and NB (318 ppm) (**c**) vapours at 25 °C (λ_{exc} = 360 nm).

The quickness of response is also linked to the ease with which the analyte could diffuse into the interior of the film [15,21]. The stronger the electrostatic interactions occurring between the NAC and the fluorophore donor sites, the slower the diffusion rate. As shown before, the binding energy associated with the formation of host-guest complexes of Calix-PPE-CBZs models with TNT is much larger than that of BQ (cf. Table 2), meaning that the overall quenching will be slowed down in the case of TNT due to the higher magnitude of the binding equilibrium successively established at each interaction site while travelling into the deeper regions of the film.

Another factor influencing the sensing performance of a given fluorophore is the thickness of the fabricated films, which usually shows a close interdependence with the last discussed parameter (electrostatic interactions) in terms of the observed response. Hence, the influence of film thickness on the quenching efficiency was evaluated for Calix-PPE-2,7-CBZ with TNT and 2,4-DNT as analytes. Moving from the thicker films (≈20 nm), used so far in the above experiments, to thinner ones (≈4 nm),

a remarkable increase in response to TNT vapours was achieved, shifting from less than 10% to over 40% in the first 30 s (Figure 4). Since the analyte equilibrium concentration is the same, as well as its diffusion rate and the microscopic binding constants, the result can be explained by the enhanced number of fluorescent sites the analyte can reach during the exposure period. In other words, the total amount of quenching events in a film of 4 nm thickness, which roughly corresponds to having only 3 stacked polymer chains, will be much larger than that reachable in a 20 nm film (ca. 15 packed chains) for the same period of time. This effect is more pronounced for TNT than for 2,4-DNT (a rise from 66% to 71% was observed) because in the latter the response is already high in the thicker film due to the higher vapour pressure and rate of diffusion of the analyte.

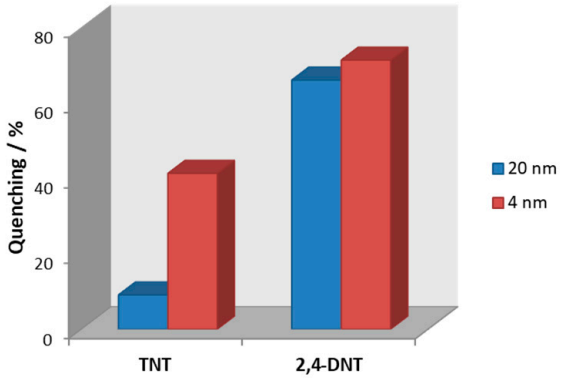

Figure 4. Effect of different thicknesses (≈4 nm and 20 nm) of Calix-PPE-2,7-CBZ thin-films on the fluorescence quenching responses to saturated TNT and 2,4-DNT vapours, upon 30 s exposure at 25 °C (λ_{exc} = 360 nm).

Similar findings related to the last effect have been previously observed and rationalised [44]. For example, 2.5 nm thin-films of pentiptycene-based polymers showed much higher sensitivity to TNT (50% quenching) and 2,4-DNT (91% quenching) in 30 s exposures when compared to thicker films [48].

To better understand the role of the calixarene moieties in promoting or enhancing the sensitivity of Calix-PPE-CBZs towards NACs, quenching studies were conducted with TBP-PPE-CBZs [31] (Chart 3), which have similar conjugated backbones but lack the calixarene units.

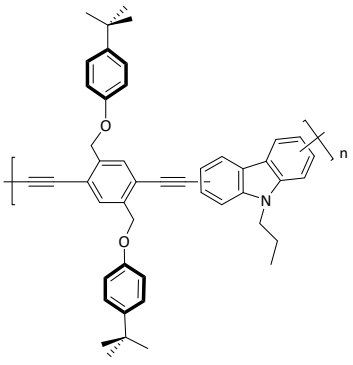

TBP-PPE-2,7-CBZ: 2,7-linkage on CBZ
TBP-PPE-3,6-CBZ: 3,6-linkage on CBZ

Chart 3. Chemical structure of TBP-PPE-CBZs.

Appropriate films of TBP-type polymers for the assay experiments revealed hard to make either due to their low solubility or to reduced fluorescence quantum yields while in solid state ($\Phi_F \approx 0.10$; [31]) due to self-quenching. To improve the signal-to-noise ratio, thicker films (ca. 50 nm) of

TBP-PPE-3,6-CBZ had to be prepared; for TBP-PPE-2,7-CBZ, owing to its sparing solubility, only films with ca. 15 nm of thickness could be fabricated. The time-dependent fluorescence quenching efficiencies of TBP-PPE-CBZs concerning TNT and 2,4-DNT are displayed in Figure S19. The quenching efficiencies for Calix-PPE-CBZs and TBP-PPE-CBZs are collected in Figure 5. Apparently, the much higher thickness of TBP-3,6-isomer film did not inhibit a slightly better response towards 2,4-DNT in comparison to the 2,7-isomer.

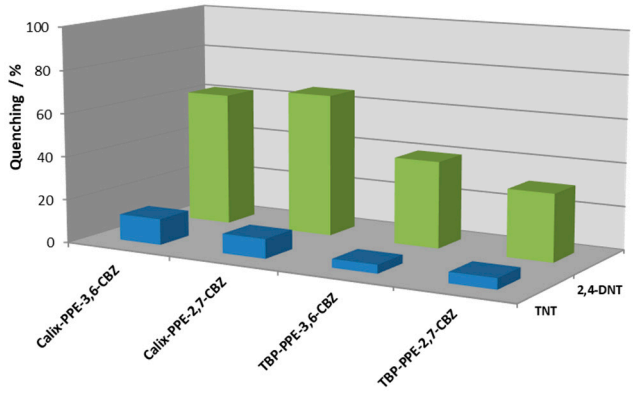

Figure 5. Fluorescence quenching responses of Calix-PPE-CBZs (20 nm thickness) and TBP-PPE-CBZs (15–50 nm thickness films; see text) upon exposure to saturated vapours of TNT and 2,4-DNT vapours (30 s) at 25 °C (λ_{exc} = 360 nm).

For both analytes, a much better performance was found for the calixarene-based polymers, where an extended three-dimensional environment is created along the stacked polymers chains, allowing for a better diffusion of the analytes through the interchain voids during a sensing event, in addition to the existence of multiple structural motifs (inside and outside the calixarene cups) for the establishment of specific interactions with a given analyte. Moreover, the Calix-PPE-CBZs also guarantee the persistence of an outstanding quantum yield in solid state for both isomers (Φ_F = 0.3–0.6; [31]) owing to the steric hindrance created by the calixarene structures around the conjugated polymer chains, which prevent their π-π stacking with the consequent self-quenching or excimer emissions.

Similarly to what was observed in the fluid phase studies, Calix-PPE-2,7-CBZ thin-films outperform their non-polymeric counterparts (Calix-2-CBZ or Calix-3-CBZ) in the detection of TNT vapours (Figure 6). For example, the emission of Calix-PPE-2,7-CBZ (4 nm thickness film) is quenched by 41% on a 30 s exposure to TNT, while the corresponding Calix-2-CBZ (1.8 nm thickness film) only reaches 31% of quenching; for the 3-isomer (same thickness), the quenching is even lower (25%). For 2,4-DNT detection, more similar values were obtained for the two types of sensing systems (71–78% of quenching after 30 s using the same film thicknesses).

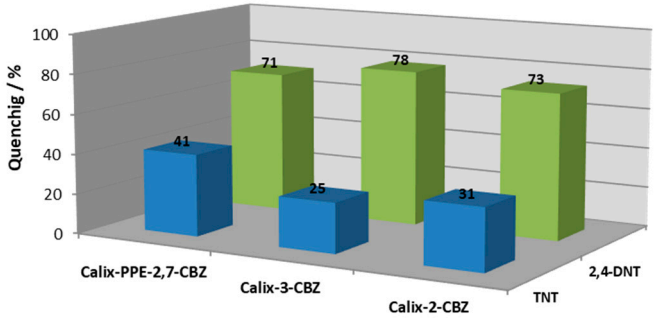

Figure 6. Fluorescence quenching responses of Calix-PPE-2,7-CBZ (4 nm films) and Calix-CBZs (1.8 nm films) upon exposure to saturated TNT and 2,4-DNT vapours for 30 s at 25 °C (λ_{exc} = 360 nm).

Preliminary experiments on the reversibility of the quenching processes revealed that, upon exposure to TNT and 2,4-DNT vapours, the emission intensities of Calix-PPE-2,7-CBZ films (≈4 nm), which were previously quenched to an extent of 82 and 88%, respectively, after 15 min of exposure, partially recovered to 34 and 42% of their pristine emissions after vacuum drying at 50 °C for 1 h. On further exposure to hydrazine vapours [49,50] the fluorescence of the films gradually recovered (Figure S20); in the case of TNT, around 80% of the original emission intensity was regained after 15 min, while for 2,4-DNT, for the same period, the final emission was even higher than that of the original film used in the assay (an increase around 25%). This fluorescence enhancement may have its origin on a substantial decrease of the number of pre-existing oxidized traps along the polymer chain upon treatment with hydrazine, a strong reducing agent. Reduction of these oxidised sites decreases the number of non-radiative decay processes. As a corollary, the fluorescence quantum yield of the polymer is enhanced. This rationale was corroborated by exposing pristine films of Calix-PPE-2,7-CBZ (ca. 2 nm thickness) to hydrazine vapours. As shown in Figure S21, emission intensities steadily increase with the time of exposure until stabilization is reached (around 20 min). Quite remarkable emission enhancements were registered. Indeed, and only after 2 min of exposure to saturated hydrazine vapours, a 58% increment of the pristine emission was observed. For prolonged exposure times (e.g., 15 min) an 85% increase was reached. The origin of this fluorescence turn-on effect may be explained by the same arguments presented above. The foregoing results suggest the potential reusability of the films in practical sensor devices.

4. Conclusions

The ability of two calix[4]arene-based carbazole-containing conjugated polymers (Calix-PPE-CBZs) to be used as fluorescence-based sensory materials for detection of nitroaromatic compounds used as explosive materials was investigated in solution and vapour phases. The studied polymers have excellent photochemical stability and high quantum yields (solution and solid state) and film-forming properties. They have shown noteworthy sensitivity and selectivity towards NACs (e.g., PA, TNT, 2,4-DNT and NB) detection in liquid phase, as determined using the static Stern-Volmer constants. A photo-induced electron transfer mechanism was evoked to rationalise the quenching processes, which was supported by the magnitude of the thermodynamically-allowed electronic transitions from the singlet excited state of model pentamers to the low-lying LUMOs of the analytes, as calculated using DFT methods. Moreover, the relative strength of electrostatic interactions developed at the ground state between Calix-2-CBZ models and the analytes were also corroborated using DFT calculations on the binding energies of the putative complexes.

The rationale underlying the observed sensitivity and selectivity of Calix-PPE-CBZs towards the explosive materials was credited to the bis-calix[4]arene motifs standing as side chains of arylene-ethynylene-carbazolylene repeating units, which provide multiple sites, inside and outside of the macrocyclics, for development of specific interactions (CH-π and π-π types) with the analytes, and to the inherent electron-donating ability of carbazole moieties along the polymer backbone, overall making the whole system a very attractive host system for electron-deficient guests. Furthermore, in solid state, the conformationally rigid three-dimensionality of calix[4]arene units disposed along the polymer chain create a network of interstitial voids that likely have allowed a smooth diffusion of the analytes throughout the films until a binding site was reached. As a corollary, better levels of detection of TNT and 2,4-DNT vapours were obtained with Calix-PPE-CBZs in comparison to TBP-PPE-CBZs.

Strong amplification effects due to excitonic migration in solid state, expected for fluorophores wired in series, were not observed. Actually, although the sensing responses of thin-films (4 nm thickness) of Calix-PPE-2,7-CBZ towards TNT are better than those of the non-polymeric Calix-CBZs films (1.8 nm), they are of similar magnitude to 2,4-DNT. This may be attributed to the low conjugation length of the synthesized polymer (M_n = 9000 g·mol^{-1}; DP ≈ 5), which may have hampered a stronger amplification of the transduction signal. Further work will be needed to enlighten this issue.

Supplementary Materials: The following items are available online at http://www.mdpi.com/2227-9040/8/4/128/s1: Synthesis and structural characterisation data of Calix-PPE-CBZs (Scheme S1, Figures S1–S3); Computational studies (Figures S4–S10); UV-Vis spectra of NACs (Figure S11); Fluorescence titration data in solution (Figures S12–S16); Limit of detection of NACs in solution (Table S1); Fluorescence titration data in solid state (Figures S17–S19); Fluorescence recovery data (Figures S20 and S21).

Author Contributions: Conceptualization, J.V.P.; methodology, J.V.P.; formal analysis, J.V.P.; investigation, P.D.B., J.V.P.; resources, J.V.P.; validation, P.D.B.; writing—original draft preparation, P.D.B.; writing—review and editing, J.V.P. All authors have read and agreed to the published version of the manuscript.

Funding: We are grateful to Fundação para a Ciência e a Tecnologia/Ministério da Ciência, Tecnologia e Ensino Superior (FCT/MCTES) for financial support (UIDB/00616/2020 and UIDP/00616/2020).

Conflicts of Interest: The authors declare no conflict of interest.

References

1. Salinas, Y.; Martínez-Máñez, R.; Marcos, M.D.; Sancenón, F.; Costero, A.M.; Parra, M.; Gil, S. Optical chemosensors and reagents to detect explosives. *Chem. Soc. Rev.* **2012**, *41*, 1261–1296. [CrossRef]
2. Germain, M.E.; Knapp, M.J. Optical explosives detection: From color changes to fluorescence turn-on. *Chem. Soc. Rev.* **2009**, *38*, 2543–2555. [CrossRef]
3. Martelo, L.M.; Marques, L.F.; Burrows, H.D.; Berberan-Santos, M.N. Explosives detection: From sensing to response. In *Fluorescence in Industry*; Pedras, B., Ed.; Springer Series on Fluorescence (Methods and Applications); Springer: Cham, Switzerland, 2019; Volume 18. [CrossRef]
4. Sun, X.; Wang, Y.; Lei, Y. Fluorescence based explosive detection: From mechanisms to sensory materials. *Chem. Soc. Rev.* **2015**, *44*, 8019–8061. [CrossRef]
5. Moore, D.S. Instrumentation for trace detection of high explosives. *Rev. Sci. Instum.* **2004**, *75*, 2499–2512. [CrossRef]
6. Moore, D.S. Recent advances in trace explosives detection instrumentation. *Sens. Imaging* **2007**, *8*, 9–38. [CrossRef]
7. Meaney, M.S.; McGuffin, V.L. Luminescence-based methods for sensing and detection of explosives. *Anal. Bioanal. Chem.* **2008**, *391*, 2557–2576. [CrossRef]
8. Sengottuvelu, D.; Kachwal, V.; Raichure, P.; Raghav, T.; Laskar, I.R. Aggregation-Induced Enhanced Emission (AIEE)-Active Conjugated Mesoporous Oligomers (CMOs) with improved quantum yield and low-cost detection of a trace amount of nitroaromatic explosives. *ACS Appl. Mater. Interfaces* **2020**, *12*, 31875–31886. [CrossRef]
9. Rasheed, T.; Nabeel, F.; Rizwan, K.; Bilal, M.; Hussain, T.; Shehzad, S.A. Conjugated supramolecular architectures as state-of-the-art materials in detection and remedial measures of nitro based compounds: A review. *Trends Anal. Chem.* **2020**, *129*, 115958. [CrossRef]
10. Rochat, S.; Swager, T.M. Conjugated amplifying polymers for optical sensing applications. *Appl. Mater. Interfaces* **2013**, *5*, 4488–4502. [CrossRef]
11. Thomas III, S.W.; Joly, G.D.; Swager, T.M. Chemical sensors based on amplifying fluorescent conjugated polymers. *Chem. Rev.* **2007**, *107*, 1339–1386. [CrossRef]
12. Toal, S.J.; Trogler, W.C. Polymer sensors for nitroaromatic explosives detection. *J. Mater. Chem.* **2006**, *16*, 2871–2883. [CrossRef]
13. Zhou, Q.; Swager, T.M. Fluorescent chemosensors based on energy migration in conjugated polymers: The molecular wire approach to increased sensitivity. *J. Am. Chem. Soc.* **1995**, *117*, 12593–12602. [CrossRef]
14. Zhou, Q.; Swager, T.M. Method for enhancing the sensitivity of fluorescent chemosensors: Energy migration in conjugated polymers. *J. Am. Chem. Soc.* **1995**, *117*, 7017–7018. [CrossRef]
15. Yang, J.S.; Swager, T.M. Fluorescent porous polymer films as TNT chemosensors: Electronic and structural effects. *J. Am. Chem. Soc.* **1998**, *120*, 11864–11873. [CrossRef]
16. Zhao, D.; Swager, T.M. Sensory responses in solution vs. solid state: A fluorescence quenching study of Poly(iptycenebutadiynylene)s. *Macromolecules* **2005**, *38*, 9377–9384. [CrossRef]
17. Thomas, S.W.; Amara, J.P.; Bjork, R.E.; Swager, T.M. Amplifying fluorescent polymer sensors for the explosives taggant 2,3-dimethyl-2,3-dinitrobutane (DMNB). *Chem. Commun.* **2005**, 4572–4574. [CrossRef] [PubMed]

18. He, G.; Yan, N.; Yang, J.Y.; Wang, H.Y.; Ding, L.P.; Yin, S.W.; Fang, Y. Pyrene-containing conjugated polymer-based fluorescent films for highly sensitive and selective sensing of TNT in aqueous medium. *Macromolecules* **2011**, *44*, 4759–4766. [CrossRef]
19. Rose, A.; Zhu, Z.G.; Madigan, C.F.; Swager, T.M.; Bulovic, V. Sensitivity gains in chemosensing by lasing action in organic polymers. *Nature* **2005**, *434*, 876–879. [CrossRef]
20. Saxena, K.; Kumar, P.; Jain, V.K. Fluorescence quenching studies of conjugated polymer poly[2-methoxy-5-(3′,7′-dimethyloctyloxy)-1,4-phenylenevinylene in the presence of TNT. *J. Lumin.* **2010**, *130*, 2260–2264. [CrossRef]
21. Nie, H.R.; Zhao, Y.; Zhang, M.; Ma, Y.G.; Baumgarten, M.; Mullen, K. Detection of TNT explosives with a new fluorescent conjugated polycarbazole polymer. *Chem. Commun.* **2011**, *47*, 1234–1236. [CrossRef]
22. Kaleeswaran, D.; Vishnoi, P.; Kumar, S.; Chithiravel, S.; Walawalkar, M.G.; Krishnamoorthy, K.; Murugavel, R. Alkyl-chain-separated triphenybenzene—Carbazole conjugates and their derived polymers: Candidates for sensory, electrical and optical materials. *Chem. Sel.* **2016**, *1*, 6649–6657. [CrossRef]
23. Asfari, Z.; Böhmer, V.; Harrowfield, J.; Vicens, J. (Eds.) *Calixarenes 2001*; Kluwer Academic: Dordrecht, The Netherlands, 2001. [CrossRef]
24. Gutsche, C.D. Calixarenes—An introduction. In *Monographs in Supramolecular Chemistry*; Stoddart, J.F., Ed.; The Royal Society of Chemistry: Cambridge, UK, 2008.
25. Kumar, R.; Sharma, A.; Singh, H.; Suating, P.; Kim, H.S.; Sunwoo, K.; Shim, I.; Gibb, B.C.; Kim, J.S. Revisiting fluorescent calixarenes: From molecular sensors to smart materials. *Chem. Rev.* **2019**, *119*, 9657–9721. [CrossRef] [PubMed]
26. Costa, A.I.; Pinto, H.D.; Ferreira, L.F.V.; Prata, J.V. Solid-state sensory properties of Calix-poly(phenylene ethynylene)s toward nitroaromatic explosives. *Sens. Actuators B Chem.* **2012**, *161*, 702–713. [CrossRef]
27. Barata, P.D.; Costa, A.I.; Prata, J.V. Calix[4]arene-carbazole-containing polymers: Synthesis and properties. *React. Funct. Polym.* **2012**, *72*, 627–634. [CrossRef]
28. Costa, A.I.; Ferreira, L.F.V.; Prata, J.V. Novel fluorescent (*p*-Phenylene ethynylene)-Calix[4]arene based polymer: Design, synthesis, and properties. *J. Polym. Sci. Part A Polym. Chem.* **2008**, *46*, 6477–6488. [CrossRef]
29. Barata, P.D.; Costa, A.I.; Ferreira, L.F.V.; Prata, J.V. Synthesis, structure, and optical properties of an alternating calix[4]arene-based meta-linked phenylene ethynylene copolymer. *J. Polym. Sci. Part A Polym. Chem.* **2010**, *48*, 5040–5052. [CrossRef]
30. Prata, J.V.; Costa, A.I.; Teixeira, C.M. A solid-state fluorescence sensor for nitroaromatics and nitroanilines based on a conjugated Calix[4]arene polymer. *J. Fluoresc.* **2020**, *30*, 41–50. [CrossRef]
31. Barata, P.D.; Prata, J.V. Cooperative effects in the detection of a nitroaliphatic liquid explosive and an explosive taggant in the vapor phase by Calix[4]arene-Based carbazole-containing conjugated polymers. *ChemPlusChem* **2014**, *79*, 83–89. [CrossRef]
32. Dennis Jr., W.H.; Rosenblatt, D.H.; Blucher, W.G.; Coon, C.L. Improved synthesis of TNT isomers. *J. Chem. Eng. Data* **1975**, *20*, 202–203. [CrossRef]
33. Borissevitch, I.E. More about the inner filter effect: Corrections of Stern–Volmer fluorescence quenching constants are necessary at very low optical absorption of the quencher. *J. Lumin.* **1999**, *81*, 219–224. [CrossRef]
34. Lakowicz, J.R. *Principles of Fluorescence Spectroscopy*, 3rd ed.; Springer: New York, NY, USA, 2006; p. 282, ISBN 978-0387-31278-1.
35. Kruse, H.; Goerigk, L.; Grimme, S. Why the standard B3LYP/6-31G* Model chemistry should not be used in DFT calculations of molecular thermochemistry: Understanding and correcting the problem. *J. Org. Chem.* **2012**, *77*, 10824–10834. [CrossRef] [PubMed]
36. Shao, Y.; Gan, Z.; Epifanovsky, E.; Gilbert, A.T.B.; Wormit, M.; Kussmann, J.; Lange, A.W.; Behn, A.; Deng, J.; Feng, X.; et al. Advances in molecular quantum chemistry contained in the Q-Chem 4 program package. *Mol. Phys.* **2015**, *113*, 184–215. [CrossRef]
37. *Spartan'18*; Wavefunction Inc.: Irvine, CA, USA, 2019.
38. Long, G.L.; Winefordner, J.D. Limit of detection a closer look at the IUPAC definition. *Anal. Chem.* **1983**, *55*, 712A–724A. [CrossRef]
39. Costa, A.I.; Prata, J.V. Unpublish results for NACs' K_{SV}, 2014.

40. Teixeira, C.M. New Molecular Receptors Based on calix[4]arenes—Application to Sensorial Chemistry. Master's Thesis, Instituto Superior de Engenharia de Lisboa, Instituto Politécnico de Lisboa, Lisboa, Portugal, 2013. Available online: http://hdl.handle.net/10400.21/3307 (accessed on 5 October 2020).
41. Barata, P.D.; Prata, J.V. New entities for sensory chemistry based on Calix[4]arene-Carbazole conjugates: From synthesis to applications. *Supramol. Chem.* **2013**, *25*, 782–797. [CrossRef]
42. Goodpaster, J.V.; McGuffin, V.L. Fluorescence quenching as an indirect detection method for nitrated explosives. *Anal. Chem.* **2001**, *73*, 2004–2011. [CrossRef]
43. Ewing, R.G.; Waltman, M.J.; Atkinson, D.A.; Grate, J.W.; Hotchkiss, P.J. The vapor pressures of explosives. *Trends. Anal. Chem.* **2013**, *42*, 35–48. [CrossRef]
44. Wang, Z.H.; Wang, Z.Y.; Ma, J.J.; Bock, W.J.; Ma, D.G. Effect of film thickness, blending and undercoating on optical detection of nitroaromatics using fluorescent polymer films. *Polymer* **2010**, *51*, 842–847. [CrossRef]
45. Lynch, E.J.; Wilke, C.R. Vapor pressure of nitrobenzene at low temperatures. *J. Chem. Eng. Data* **1960**, *5*, 300. [CrossRef]
46. Pella, P.A. Measurement of the vapor pressures of TNT, 2,4-DNT, 2,6-DNT, and EGDN. *J Chem Thermodyn.* **1977**, *9*, 301–305. [CrossRef]
47. Emel'yanenko, V.N.; Varfolomeev, M.A.; Novikov, V.B.; Turovtsev, V.V.; Orlov, Y.D. Thermodynamic properties of 1,4-Benzoquinones in gaseous and condensed phases: Experimental and theoretical studies. *J. Chem. Eng. Data* **2017**, *62*, 2413–2422. [CrossRef]
48. Yang, J.S.; Swager, T.M. Porous shape persistent fluorescent polymer films: An approach to tnt sensory materials. *J. Am. Chem. Soc.* **1998**, *120*, 5321–5322. [CrossRef]
49. Thomas, S.W.; Swager, T.M. Trace hydrazine detection with fluorescent conjugated polymers: A turn-on sensory mechanism. *Adv. Mater.* **2006**, *18*, 1047–1050. [CrossRef]
50. Naddo, T.; Che, C.; Zhang, W.; Balakrishnan, K.; Yang, X.; Yen, M.; Zhao, J.; Moore, J.S.; Zang, L. Detection of explosives with a fluorescent nanofibril film. *J. Am. Chem. Soc.* **2007**, *129*, 6978–6979. [CrossRef]